Chemistry and Materials Research
ISSN 2224- 3224 (Print) ISSN 2225- 0956 (Online)
Vol.10 No.6s, 2018 

# Synthesis, Corrosion Inhibition and Theoretical Studies of (E)-2-((2,5-Dichlorophenyl)diazenyl)naphthalen-1-ol as Corrosion Inhibitor of Mild Steel in 0.5 M Hydrochloric Acid

Justinah Amoko[1,3] Olawale Akinyele[2*] Dare Olayanju[2] Augustus Oluwafemi[1]
Christopher Aboluwoye[1]
1.Department of Chemical Sciences, Adekunle Ajasin University, Akungba Akoko, Nigeria
2.Department of Chemistry, Obafemi Awolowo University, Ile-Ife, Nigeria
3.Deapartment of Chemistry, Adeyemi College of Education, Ondo Nigeria

**Abstract**
The inhibitory capacity of (E)-2-((2,5-dichlorophenyl)diazenyl)naphthalen-1-ol (DPD) against mild steel corrosion in 0.5 M HCl has been studied at different temperature (25 – 65 ºC) by gravimetric and electrochemical methods. Quantum chemical study using DFT was employed to explain the experimental results. The corrosion activation energy, $E_a$, Free energy, $\Delta G^o_{ads}$, enthalpy, $\Delta H^o_{ads}$ and entropy, $\Delta S^o_{ads}$, of adsorption were calculated. The inhibition efficiency increases with increase in concentration and decreases with increasing temperature. The adsorption on the mild steel surface was found to follow Langmuir adsorption isotherm while the potentiodynamic polarization revealed DPD as the cathodic type inhibitor. The adsorption occurred via exothermic process and followed physisorption mechanism. The study therefore presented DPD as potential inhibitor of mild steel corrosion in acidic environment.
**Keywords:** Weight loss, Polarization, Kinetic parameters, Naphthol azo-dye, Inhibition efficiency

*The research is financed by the Tertiary Education Trust Fund (TET Fund)*

## 1. Introduction

Mild steel is an important alloy in industries with good mechanical strength. It consists of about 96 – 99% iron (Nagiub *et al.,* 2013; Fiori-Bimbi *et al.,* 2015) and cheaper when compare to other alloys. It is a useful material in marine applications, petroleum production and refinery, construction and metal processing equipment. On the other hand, acid solutions are used in some industrial processes involving acid pickling, acid descaling and acid cleaning (Nagiub *et al.,* 2013) which in turn pose attack on the metal(s) leading to corrosion. Corrosion is described as the loss in the strength and values of a metal owing to its chemical or electrochemical interaction with its environment (Selvaraj *et al.,* 2015). Corrosion of metals, if not checked, could amount to high cost of equipment maintenance, reduction in the useful salvage value of equipment and the overall effect will be down-time production of such industries. Therefore, prevention of metals or mild steel from corrosion is always of both theoretical and practical interest (Peme *et al.,* 2015). Organic inhibitors have gained recognition nowadays as one of the most economical means of combating corrosion (Ramachandran & Jovancicevic, 1999). They act as corrosion inhibitor by adsorbing on the mild steel surface leading to the formation of protective film (Obot *et al.,* 2009) thereby preventing further attack of the aggressive media. Their adsorption on the metal-solution interface is described as quasi-substitution process that involves gradual replacement of water molecules initially adsorbed on the metal surface by the organic molecules in the aqueous solution (Hamdy & El-Gendy, 2013). Most organic inhibitors are compounds having donor atoms such as N, S, P, O etc, pi-electron system and plane conjugated systems involving all kinds of aromatic rings in their moieties (Abdallah, 2002; Hegazy, 2009; Hasanov *et al.,* 2010). Azo-dyes with the N=N chromophoric group have been demonstrated as one of these excellent corrosion inhibitors for metal and alloys in varying media (Ebenso *et al.,* 2008; Al-Doori & Shihab, 2014; Fouda *et al.,* 2014) owing to their ability to coordinate to the metal-ions via the nitrogen of the azo group at the surface of the metal. There are various methods to corrosion inhibition study which includes the use of the gravimetric method - the simplest, oldest and the most accurate method of estimating the corrosion rate which does not involve complex equipment set-up, electrochemical methods - mostly involving three electrodes system such as the electrochemical impedance spectroscopy, potentiodynamic polarisation, electrochemical potential monitoring and electrochemical noise (Yildiz, 2015; Ateya *et al.,* 1984; Hassan, 2007) etc. Electrochemical methods of corrosion study help to give valuable information on corrosion and adsorption mechanism most especially if it involves adsorption of film or an organic coating (Zhang *et al.,* 2007; Wang *et al.,* 2011). In general, the mechanism of adsorption for most organic corrosion inhibitors are often predicted from the classical adsorption mechanism which includes the Langmuir, Frumkin, Temkin, Freundlich etc, out of which the best fit is used in the prediction of the mechanism (Durnie et al., 1999).

Quantum chemistry method of corrosion study, among others, is a promising technique to study the interfacial interaction of molecule–metal and the micro-scale inhibition mechanism (Peme *et al.,* 2015; Olasunkanmi *et al.,* 2015). It is an effective method for studying the correlation between molecular structure and

 

inhibition efficiency (Riggs & Hurd, 1967).
In this present study, (E)-2-((2,5-dichlorophenyl)diazenyl)naphthalen-1-ol (DPD) was synthesized via diazotisation and pling reactions while its inhibition efficiencies for mild steel corrosion in 0.5 M HCl were studied using both gravimetric and electrochemical methods. Density Functional theory (DFT), using Spartan 14 software, was used to give theoretical background to the experimental results.

## 2. Experimental

### 2.1 *Synthesis of (E)-2-((2,5-dichlorophenyl)diazenyl)naphthalen-1-ol (DPD)*

DPD was synthesized using the method reported in literature (Scheme 1) (Ahmadi & Amani, 2012). A suspension of 2, 5-dichloroaniline (6.48g, 40mmol) in hydrochloric acid (36 ml) and water (16 ml) was heated to around 70ºC until complete dissolution. The clear solution poured into ice was diazotized below 5ºC with sodium nitrite (2.8g, 40mmol) dissolved in water (10ml). The resulting cold diazonium solution was then added slowly with continuous vigorous stirring over the course of 45 mins at 0ºC to a solution of 1-naphthol (5.77g, 40mmol) in water (75ml) containing sodium hydroxide (1.6g) and sodium carbonate (14.8g). The product was collected by filtration and washed with water then later recrystallized from ethanol three times to give orange solid. The synthesized compound was characterized using UV-visible spectroscopy, Infra-Red spectroscopy and Nuclear Magnetic Resonance ($^{1}$HNMR and $^{13}$CNMR). Melting point: 72 – 74 ºC, yield: 75 %. FTIR (KBr, cm$^{-1}$): 3464 (-OH group), 3086 (C-H, aromatic), 1624 (C=C, aromatic), $1583_{asy}$&$1423_{sym}$ (N=N), 1521 & 1386 ($NO_{2str}$), 1084&1053 (C-$O_{str}$), 764 (C-$Cl_{str}$). UV-Vis: $\lambda_{max}$ = 284, 449 nm. $^{1}$H-NMR (DMSO): δ = 3.51 (1H, s), 7.04 (1H, d), 7.54 (1H, dd), 7.61 (1H, ddd), 7.73 (2H, m), 7.83 (1H, d), 7.97 (1H, d), 8.24 (1H, d), 8.94 (1H, d) ppm. $^{13}$C-NMR (DMSO) δ= 118, 122, 124, 125, 128, 131, 132, 139, 153 ppm.

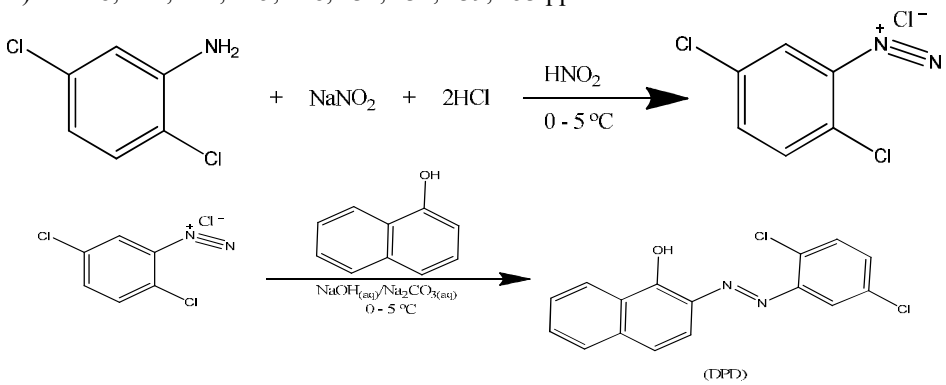


Scheme 1: Synthesis of DPD

### 2.2 *Test Solution Preparation*

0.5 M HCl was prepared using hydrochloric acid of standard grade and distilled water which was used to test the synthesized DPD. DPD was added to the acidic solution in a dosage of 10 – 50 ppm to test its inhibitory capacity on mild steel. Steel coupons for gravimetric experiment were introduced into beakers containing this tested solution while the experiment was performed in thermostated water bath at each test temperature (25, 35, 45, 55 and 65ºC) for 6 hrs.

### 2.3 *Mild Steel Pre-treatment*

Commercially available mild steel was bought and mechanically machined into dimension 3 cm x3 cm x0.05 cm with hole at the centre for easy hooking. Each were polished with evenly gritted emery paper; washed with distilled water and degreased with acetone by dipping them in acetone for five minutes and dried over $CaCl_2$ in desiccators overnight (Geethamani & Kasthuri, 2015; Nabi & Hussain, 2012).

### 2.4 *GravimetricExperiment*

The pre-treated Mild steel coupon was weighed with the aid of analytical balance (0.0001 sensitivity) and immersed in 100 ml 0.5 M HCl test solution loaded with the different concentrations of the inhibitor (10 – 50 ppm) in a beaker for 6 hours at varying temperature (25ºC – 65ºC at $10^{0}$C interval) by keeping each of the test temperature constant using a thermostatic water bath. Each sample of the mild steel was withdrawn from the test solution after 6 hrs and then brushed with brittle brush, washed with distilled water, rinsed in acetone and dried in oven for 15 mins at 40ºC before reweighing (Geethamani & Kasthuri, 2015). Each of this experiment was performed in triplicate for accurate results and the mean of the final weight was used in the calculation. From the weight loss results, the corrosion rate, $C_R$, degree of surface coverage, θ and the percentage inhibition efficiency, IE %, were determined using Equations 1, 2 and 3 respectively.

 

$$C_R = \frac{W_O - W_1}{At} \quad (1)$$

$$\theta = 1 - \frac{C_R^i}{C_R^o} \quad (2)$$

$$\%IE = \theta \times 100 \quad (3)$$

Where, $W_o$ and $W_1$ are the weight loss (g) of mild steel in the absence and presence of the inhibitor respectively. A is the area of the mild steel ($cm^2$), t is the immersion time (hrs). $C_R^i$ and $C_R^o$ are the corrosion rates (g $cm^{-2}$ $hr^{-1}$) in the presence and absence of the inhibitor respectively.

**2.5 Electrochemical measurement**:
Electrochemical experiments were conducted in a three-electrode cell using corrosion Lab and Versa stat 4 software under standard condition. A platinum sheet was used as the counter electrode (CE), saturated calomel electrode (SCE) as the reference electrode, while the mild steel machined into rectangular specimens with an exposed area of 1 $cm^2$ as the working electrode (WE). All potentials in this work are referred to the SCE (0.2412 V) with respect to the normal hydrogen electrode. Measurements were performed in naturally aerated and unstirred solutions maintained at 298 K using a thermostatic water bath. The working electrode was immersed in the test solution for 10 mins to establish a steady state open current potential (OCP). Potentiodynamic polarization studies were carried out sweeping the applied potential from -250 mV to +250 mV at OCP with a scan rate of 1$mVs^{-1}$ while the current, *I*, was recorded in the absence and presence of varying concentration of DPD (15 – 75 ppm).

**2.6 Quantum Chemical Calculations**
Quantum chemical calculations were carried out with complete geometry optimisation using Spartan 14 software by density function theory (DFT) with 6-31G* basis set for all atoms (Obi-Egbedi *et al.,* 2011). Quantum parameters such as the highest occupied molecular orbital (HOMO), lowest unoccupied molecular orbital (LUMO), Energy gap (ΔE), Electronegativity [γ], global hardness [η], global softness (α), and fraction of electrons transferred (Δμ) were acquired using the Spartan 14 software.

**3. Results and Discussion**
**3.1 Infrared Spectra of the Azo-dye**
The infrared spectrum of the synthesized azo dye exhibits a band at 3464 $cm^{-1}$ assigned to the OH vibration frequency (Ahamadi & Amani, 2012; Nabi & Hussain, 2012). Band at 3086$cm^{-1}$ was assigned to $sp^2$ CH vibration of the aromatic ring (Nabi & Hussain, 2012) while the band at 1624$cm^{-1}$ was due to the -C=C-vibration frequency. Also, the spectrum displays azo group (-N=N-) at $1583_{asy}$ and $1423_{sym}$ respectively (Anitha *et al.,* 2011; Otutu, 2013; Cabir *et al.,* 2013). The band at 754$cm^{-1}$ was due to the stretching band of C-Cl group. The IR spectrum showed the various expected characteristics bands signifying the formation of the dye.

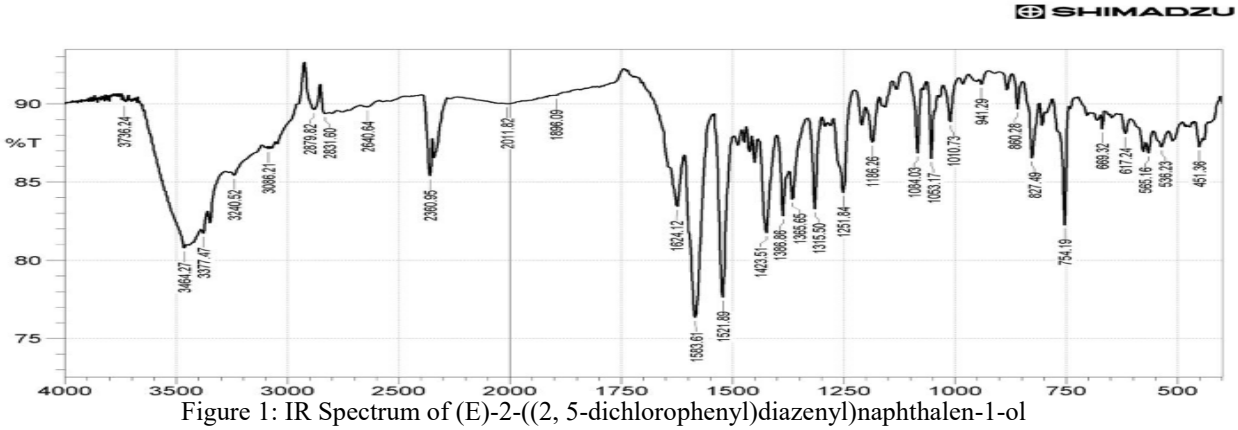

Figure 1: IR Spectrum of (E)-2-((2, 5-dichlorophenyl)diazenyl)naphthalen-1-ol

**3.2 Electronic Spectra**
Electronic absorption spectrum for the synthesized azo-dyes using ethanol (Figure 2) showed two major peaks. Peak at 284 nm due to π-π* aromatic transition and at 449 nm due to π-π* of the intermolecular charge transfer (IMCT) involving the whole molecule through the -N=N- group (Canakci *et al.,* 2014).

 

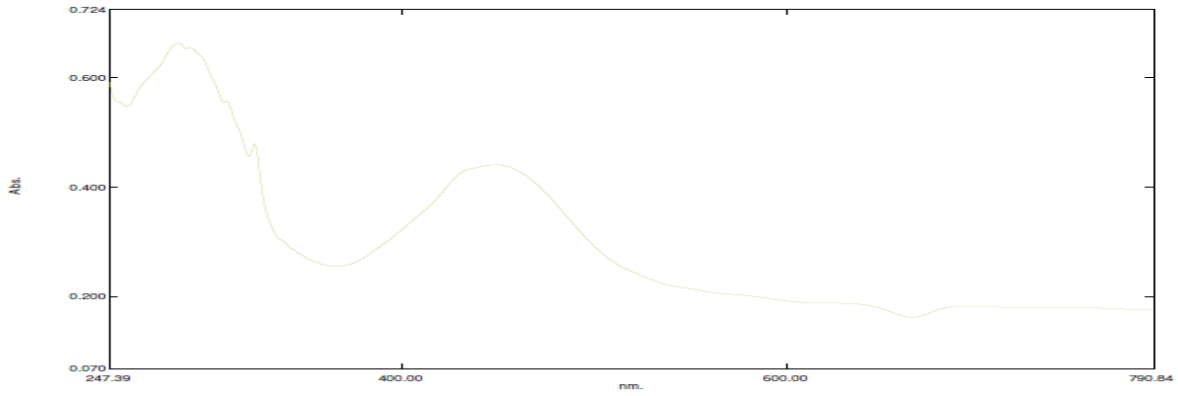


Figure 2: UV-visible Spectrum of (E)-2-((2,5-dichlorophenyl)diazenyl)naphthalen-1-ol

### 3.3 Nuclear Magnetic Spectrum ($^1$HNMR and $^{13}$CNMR)

The $^1$HNMR spectrum of the azo-dye (Figure 3(a)) was measured using d$^6$-DMSO solvent. The results showed a signal at 3.51 ppm which was assigned to the presence of proton of hydroxyl group of the naphthol and water. The same spectrum displays signal between 7.04 – 8.94 ppm attributed to the protons on the phenyl and the naphthalene rings. The signal at 2.50 ppm was due to the existence of methyl group as impurity in the compound.$^{13}$CNMR spectrum (Figure 3(b)) showed signals at 118, 122, 124, 125, 128, 131, 132, 139 and 153 ppm corresponding to the various aromatic carbons. Signals at 125 and 132 ppm, and at 139 and 153 ppm were assigned to the aromatic carbons carrying the chlorine atoms and the azo group respectively.

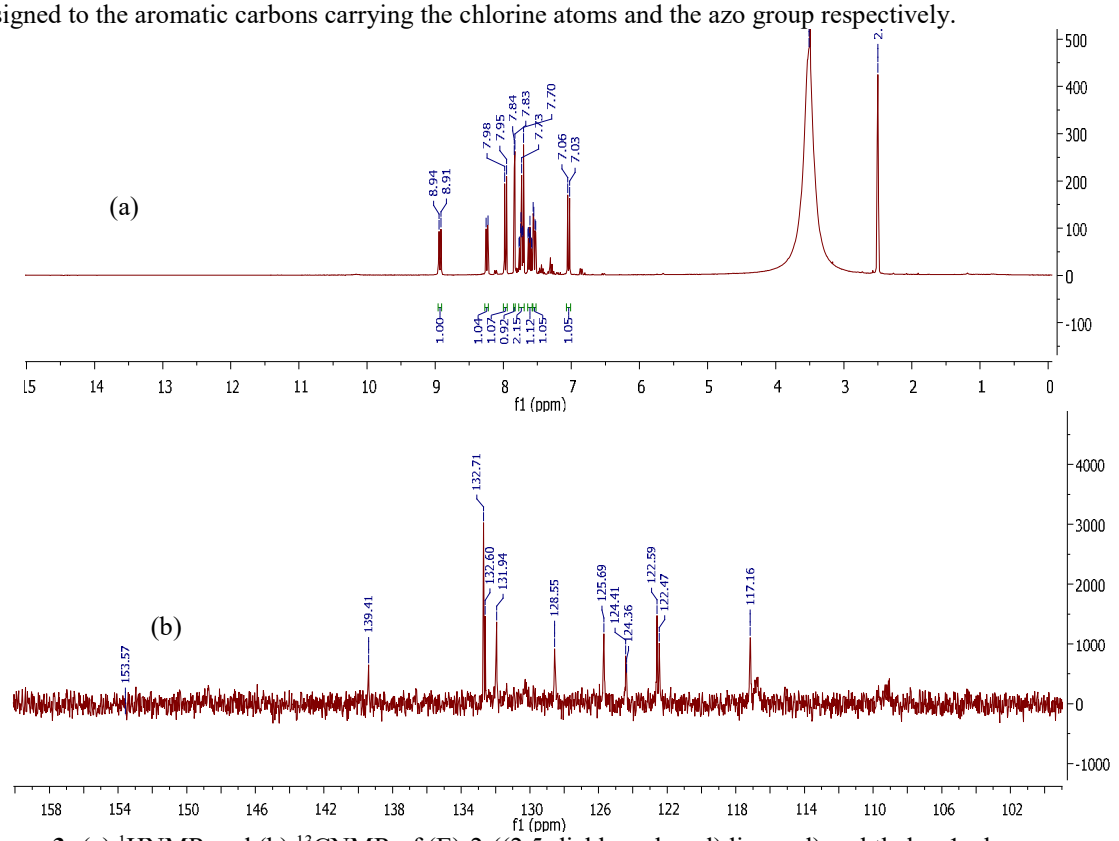


**Figure 3:** (a) $^1$HNMR and (b) $^{13}$CNMR of (E)-2-((2,5-dichlorophenyl)diazenyl)naphthalen-1-ol

All spectra data (FTIR, electronic, $^1$HNMR and $^{13}$CNMR) are in good agreement with the formation of the azo-dye.

### 3.4 Weight loss measurements

Corrosion parameters obtained from weight loss measurement for mild steel corrosion in the absence and presence of the studied azo dye at various concentration and temperature in 0.5 M HCl were summarized by Table 1 and Figure 4.

 

Table 1: Parameters obtained from Weight Loss Analysis of Mild Steel in 0.5 M HCl in the Absence and Presence of DPD

| Compound | Temp (K) | Concentration of the inhibitor (M) | Weight loss (g) | Corrosion rate($gcm^{-2}hr^{-1}$) | IE% | Θ |
|---|---|---|---|---|---|---|
| DPD | 298 | **Blank** | **0.1590** | **0.0026** | - | - |
| | | 0.000032 | 0.0640 | 0.0011 | 56 | 0.5627 |
| | | 0.000063 | 0.0540 | 0.0010 | 63 | 0.6295 |
| | | 0.000095 | 0.0491 | 0.0009 | 67 | 0.6645 |
| | | 0.000126 | 0.0440 | 0.0007 | 72 | 0.7152 |
| | | 0.000158 | 0.0350 | 0.0006 | 76 | 0.7644 |
| | 308 | **Blank** | **0.1700** | **0.0030** | - | - |
| | | 0.000032 | 0.0860 | 0.0015 | 46 | 0.4612 |
| | | 0.000063 | 0.0740 | 0.0013 | 55 | 0.5449 |
| | | 0.000095 | 0.0630 | 0.0011 | 60 | 0.5984 |
| | | 0.000126 | 0.0570 | 0.0010 | 64 | 0.6422 |
| | | 0.000158 | 0.0500 | 0.0009 | 69 | 0.6927 |
| | 318 | **Blank** | **0.2890** | **0.0050** | - | - |
| | | 0.000032 | 0.1590 | 0.0030 | 40 | 0.4022 |
| | | 0.000063 | 0.1550 | 0.0028 | 45 | 0.4525 |
| | | 0.000095 | 0.1300 | 0.0024 | 52 | 0.5178 |
| | | 0.000126 | 0.1160 | 0.0021 | 59 | 0.5861 |
| | | 0.000158 | 0.0930 | 0.0018 | 65 | 0.6509 |
| | 328 | **Blank** | **0.4000** | **0.0068** | - | - |
| | | 0.000032 | 0.2700 | 0.0049 | 28 | 0.2807 |
| | | 0.000063 | 0.2200 | 0.0039 | 42 | 0.4184 |
| | | 0.000095 | 0.2030 | 0.0037 | 46 | 0.4562 |
| | | 0.000126 | 0.1910 | 0.0034 | 50 | 0.4996 |
| | | 0.000158 | 0.1600 | 0.0029 | 57 | 0.5697 |
| | 338 | **Blank** | **0.8060** | **0.0135** | - | - |
| | | 0.000032 | 0.5920 | 0.0106 | 22 | 0.2183 |
| | | 0.000063 | 0.5640 | 0.0094 | 30 | 0.3001 |
| | | 0.000095 | 0.5160 | 0.0087 | 36 | 0.3558 |
| | | 0.000126 | 0.4590 | 0.0082 | 39 | 0.39108 |
| | | 0.000158 | 0.4330 | 0.0074 | 45 | 0.44982 |

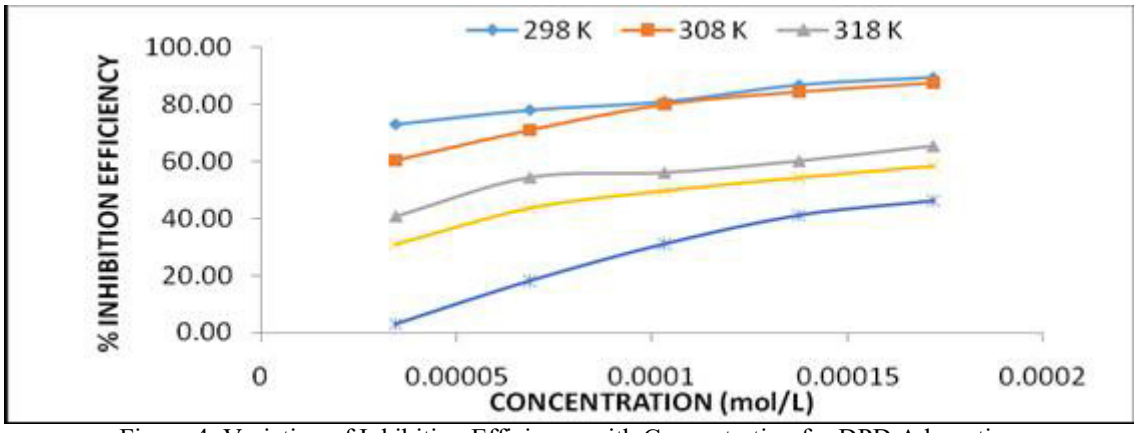


Figure 4: Variation of Inhibition Efficiency with Concentration for DPD Adsorption

 

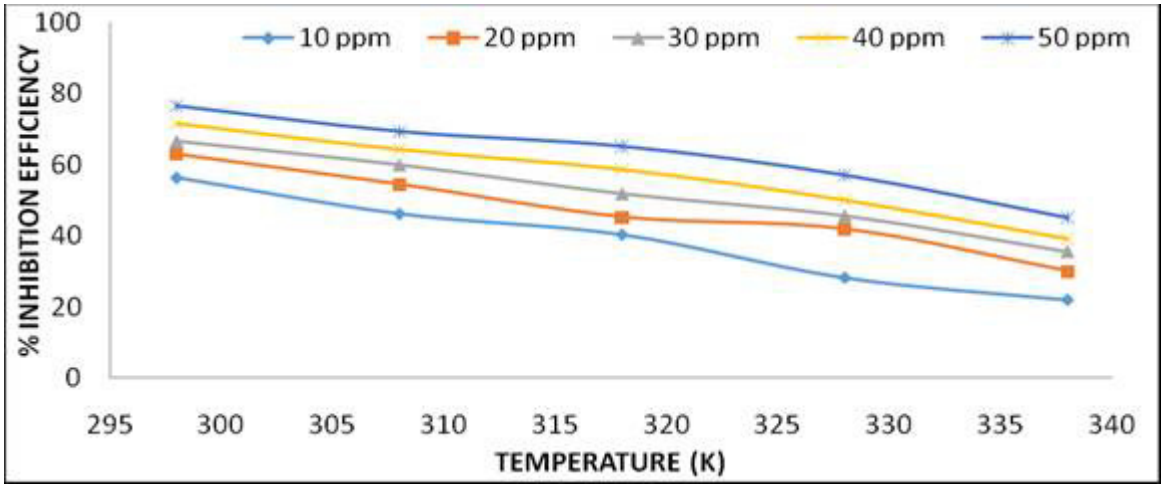


Figure 5: Variation of Inhibition Efficiency with Temperature for DPD Adsorption

Table 1 showed that the corrosion rate decreases with increase in the concentration of the inhibitor and increases with the increase in tested temperature. This may be due to the fact that as the concentration of the inhibitor increases, more of its molecules are adsorbed on the metal surface thereby causing more active site to be blocked by the inhibitor resulting in reduction of the corrosion rate. More so, as the temperature increases, it becomes easier for the already adsorbed DPD molecules to desorb from the surface of the mild steel. Similar observations have been reported in literature for the adsorption of some organic compound on the surface of metal (Deng & Li, 2012; Qian *et al.,* 2013). Figure 4 shows that as the concentration of DPD increases, the inhibition efficiency increases. This behaviour could be attributed to the increase in the rate of adsorption of the inhibitor molecule on the metal surface as the concentration increases thereby preventing further attack by the aggressive medium (Obot *et al.,* 2009). While, Figure 5 shows that the inhibition efficiency of DPD for mild steel corrosion in 0.5 M HCl decreases with increase in the experimental temperature due to increase in the rate of DPD desorption as the experimental temperature increases.

### 3.5 Tafel Polarization Measurements

The polarization curves of the mild steel used in 0.5 M HCl solution in the absence and presence of different concentrations of DPD are shown in Figure 6. Other parameters like the corrosion potential ($E_{corr}$), corrosion current density ($I_{corr}$), anodicTafel slope ($\beta_a$), cathodic Tafel slope ($\beta_c$) and percentage inhibition efficiency (% IE) are summarized in Table 2. The inhibition efficiency is calculated from the value of corrosion current density, which was evaluated from extrapolation method, using equation 4 (He *et al.,* 2014).

$$\%IE = \frac{I^{o}_{corr} - I_{corr}}{I^{o}_{corr}} \times 100 \qquad 4$$

Where, $I^{o}_{corr}$ and $I_{corr}$ are the corrosion densities in the absence and presence of the inhibitor respectively.

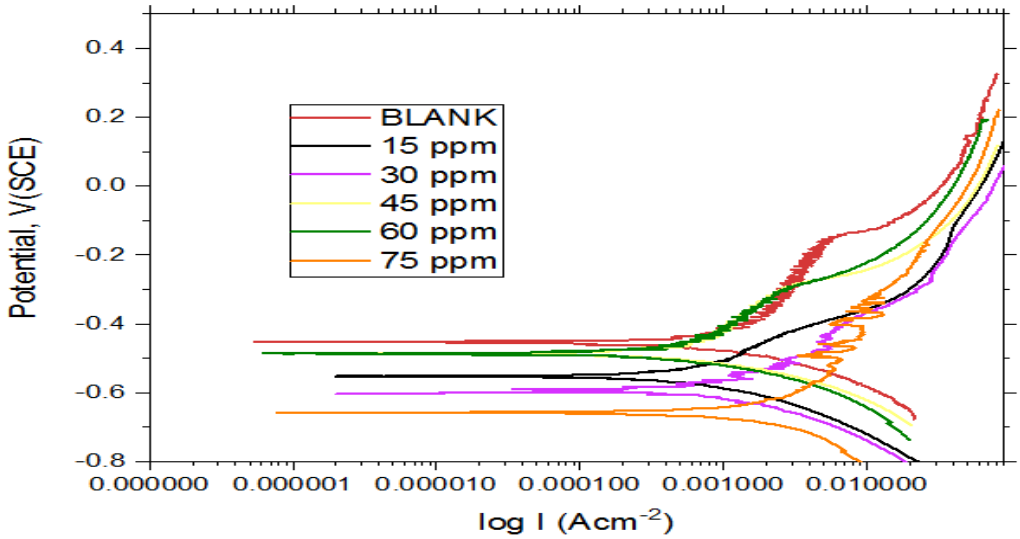


Figure 6: Polarization Curve for the Mild Steel in 0.5M HCl in absence and presence of DPD

 

Table 2: Polarization Parameters and Inhibition Efficiencies for Mild Steel in 0.5 M HCl solution in the absence and presence of different Concentrations of DPD at 298 K

| Compd | Conc (g) | $-\beta_c$ (mV/decade) | $\beta_a$ (mV/decade) | $C_R$mpy | $-E_{corr}$(mV) | $I_{corr}$ (μmA) | % IE |
|---|---|---|---|---|---|---|---|
| DPD | Blank | 111.71 | 292.71 | 461.40 | 451.4 | 1.009000 | - |
| | 0.015 | 149.75 | 167.86 | 364.97 | 544.3 | 0.798906 | 20.82 |
| | 0.030 | 85.50 | 156.26 | 336.58 | 599.0 | 0.736771 | 26.82 |
| | 0.045 | 73.68 | 157.88 | 146.12 | 478.2 | 0.319862 | 68.29 |
| | 0.060 | 76.41 | 170.34 | 136.26 | 299.1 | 0.299134 | 70.35 |
| | 0.075 | 31.37 | 217.47 | 128.13 | 664.9 | 0.280482 | 72.20 |

Generally, organic inhibitors can be classified as cathodic, anodic or mixed-type inhibitor depending on whether there is decrease in the corrosion current densities at the cathodic or anodic or both sides, respectively, of the Tafel curve on addition of the inhibitor (Hu *et al.,* 2013; Quraishi, 2013). It could be observed from Figure 6, that the cathodic corrosion current densities decrease considerably on addition of DPD to the corrosive medium giving an indication that DPD is a cathodic type inhibitor. At the same time, $E_{corr}$ are displaced to the more negative values at the cathodic side. This suggests that the inhibitor has retarding effect on the cathodic half corrosion reaction, which works mainly by increasing the hydrogen evolution potential in the HCl solution, thereby shifting the corrosion potential to more negative values and slows the cathodic process of the alloy. Hence, the corrosion reaction of the mild steel is inhibited.

The cathodic polarization curves equally give rise to almost parallel Tafel lines, an indication that the addition of DPD does not modify the mechanism of the hydrogen evolution reaction process (He *et al.,* 2014) but inhibited the corrosion reaction only by blocking the reaction sites without affecting the actual reaction mechanism (He *et al.,* 2014, Hu *et al.,* 2013; Farag & Hegazy, 2013; Qian *et al.,* 2013). Table 2 shows that the inhibition efficiency of DPD increases up to 72.20 % with the increase in its concentration up to 0.075 g suggesting that DPD can obviously inhibit the corrosion of mild steel in 0.5 M HCl solution, and better inhibition efficiencies are obtained at higher concentrations.

### 3.6 Adsorption consideration

The adsorption interaction between an organic inhibitor and the metal surface can be explained using some classical adsorption isotherms. In this present study, the adsorption of DPD on mild steel surface was observed to obey Langmuir adsorption isotherm (Equation 5) (Deng and Li, 2012; Li *et al.,* 2010).

$$C/\theta = \left[1/K_{ads}\right] + C \qquad 5$$

Where, $C$ is the concentration of inhibitor, $K_{ads}$ the equilibrium adsorption constant and $\Theta$ the extent of surface coverage. A plot of C/$\Theta$ against C at different temperatures (298 – 338 K) were made and the corresponding parameters obtained from this plots are listed in Table 3.

Fig 7 shows the straight lines of C/O versus C at 298 – 338 K. Both linear correlation coefficients (R) and slope values are closer to 1, suggesting that the adsorption of DPD on Mild steel surface obeys Langmuir adsorption isotherm. The little deviation from unity observed in the slope may be due to the repulsion force in the adsorption layer (Mu *et al.,* 2006).

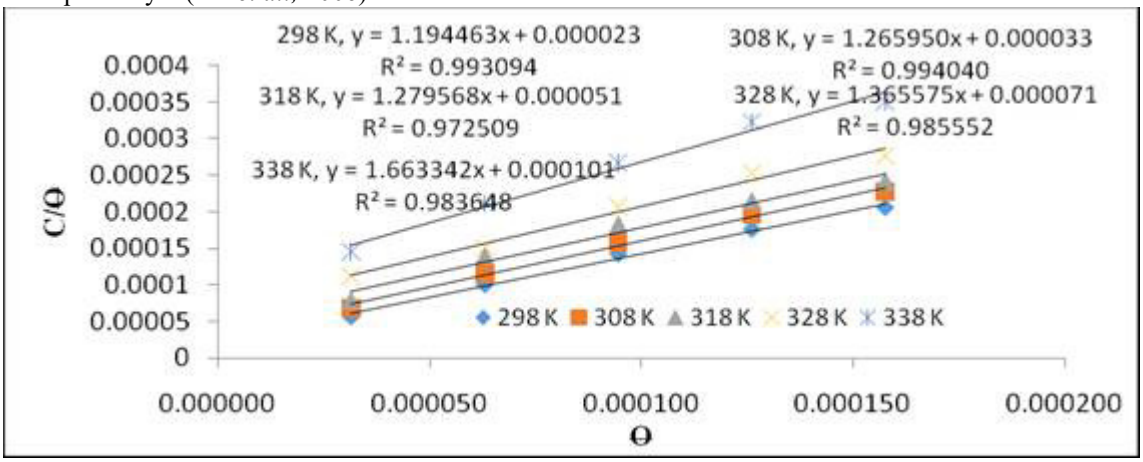


Figure 7: Langmuir Adsorption Isotherm for DPD Adsorption in 0.5 M HCl at different Concentrations of DPD

The decrease in the adsorptive equilibrium constant ($K_{ads}$) value with increase in temperature indicated that at relatively lower temperature, DPD molecules were easily and strongly adsorbed onto the mild steel surface.

 

On the other hand, a rise in the experimental temperature causes the adsorbed inhibitors to desorb from the mild steel surface (Deng and Li, 2012). Using the adsorptive equilibrium constant ($K_{ads}$) values, thermodynamic parameters were calculated in order to further elucidate the adsorption process of DPD on the mild steel surface. The standard Gibb's free energies of adsorption ($\Delta G^o_{ads}$) were calculated using equation 6 (Tu *et al.,* 2012).

$$K_{ads} = \frac{1}{55} \ell^{\frac{-\Delta G^o_{ads}}{RT}} \quad 6$$

Where R is the universal gas constant, $\Delta G^o_{ads}$ is the free energy of adsorption and 55.5 is the molar concentration of water in the solution. $\Delta G^o_{ads}$ is related to the enthalpy, $\Delta H^o_{ads}$ and entropy, $\Delta S^o_{ads}$, of adsorption by equation 7.

$$\Delta G^o_{ads} = \Delta H^o_{ads} - T\Delta S^o_{ads} \quad 7$$

A plot in form of $\Delta G^o_{ads}$ versus T (Figure 8) gave a straight line with change in standard adsorption enthalpy, $\Delta H^o_{ads}$ as the intercept and change in standard adsorption entropy, $\Delta S^o_{ads}$ as the slope (Fiori-Bimbi *et al.,* 2015). Intercept and slope of this plot yielded $\Delta H^o_{ads}$ of -31.227 kJ mol$^{-1}$ and $\Delta S^o_{ads}$ of +0.017 kJ mol$^{-1}$K$^{-1}$, respectively (Table 3).

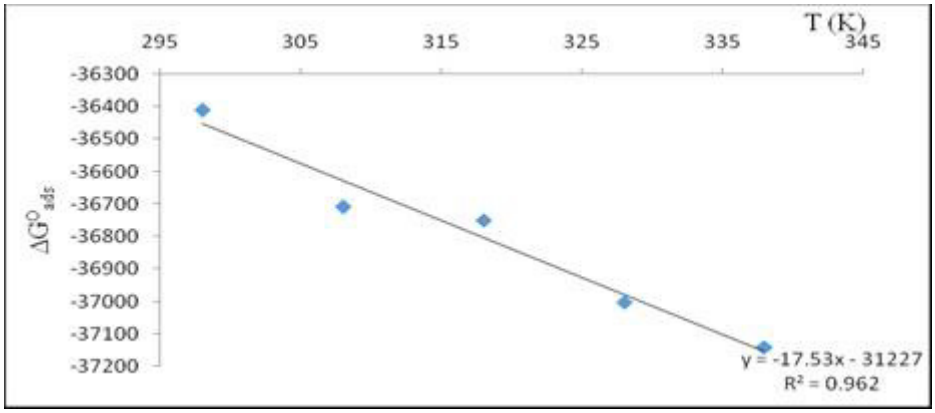


Figure 8: Determination of the Enthalpy, $\Delta H^o_{ads}$ and Entropy, $\Delta S^o_{ads}$, of Adsorption of DPD on the Mild Steel Surface in 0.5 M HCl.

Table 3: Values from Langmuir Adsorption Isotherm and Thermodynamics Study

| | Langmuir | | | | Thermodynamics parameters | | |
|---|---|---|---|---|---|---|---|
| | T (K) | $R^2$ | $1/K_{ads}$ | $K_{ads}$ | $\Delta G^o_{ads}$(kJmol$^{-1}$) | $\Delta S^o_{ads}$ (kJ mol$^{-1}$K$^{-1}$) | $\Delta H^o_{ads}$ (kJ/mol) |
| DPD | 298 | 0.993 | 0.000023 | 43478.26 | -36411.4 | | |
| | 308 | 0.994 | 0.000033 | 30303.03 | -36708.8 | 17.533 | -31227 |
| | 318 | 0.972 | 0.000051 | 19607.84 | -36749.7 | | |
| | 328 | 0.986 | 0.000071 | 14084.51 | -37003.1 | | |
| | 338 | 0.984 | 0.000101 | 9900.99 | -37140.9 | | |

Negative values of $\Delta G^o_{ads}$ indicated a spontaneous adsorption process. In general, value of $\Delta G^o_{ads}$ around -20 kJmol$^{-1}$ indicates physical adsorption and value of $\Delta G^o_{ads}$ of -40 kJ/mol and above indicates chemisorption (Solmaz *et al.,* 2008). In this study, values of $\Delta G^o_{ads}$ obtained were in the range -36.41 to -37.82 kJ/mol which gave a hint of complex adsorption mechanism. The positive value of $\Delta S^o_{ads}$ could be due to desorption of water molecules from the surface and increase in solvent entropy. Negative value of $\Delta H^o_{ads}$ obtained indicated the exothermic nature of the adsorption process (Fiori-Bimbi *et al.,* 2015). In an exothermic process physisorption can be differentiated from chemisorption using the value of $\Delta H^o_{ads}$. For chemisorption process $\Delta H^o_{ads}$ approaches -100 kJmol$^{-1}$ while, for physisorption, $\Delta H^o_{ads}$ tends to -40 kJmol$^{-1}$. -31.227 kJmol$^{-1}$ obtained for $\Delta H^o_{ads}$ in this work gives an idea of physical adsorption.

### 3.7 Kinetic Studies and Activation Parameters

Kinetic model was used to explain the behaviour of DPD. The apparent activation energies, $E_a$, for the corrosion process and the pre-exponential factors, $A$, were estimated from Arrhenius equation (Equation 8) using the slopes and intercepts from the Arrhenius plots (Figure 9) respectively (Tu *et al.,* 2012) and the values are presented in Table 4.

$$\ln C_R = \ln A - \frac{E_a}{RT} \quad 8$$

 

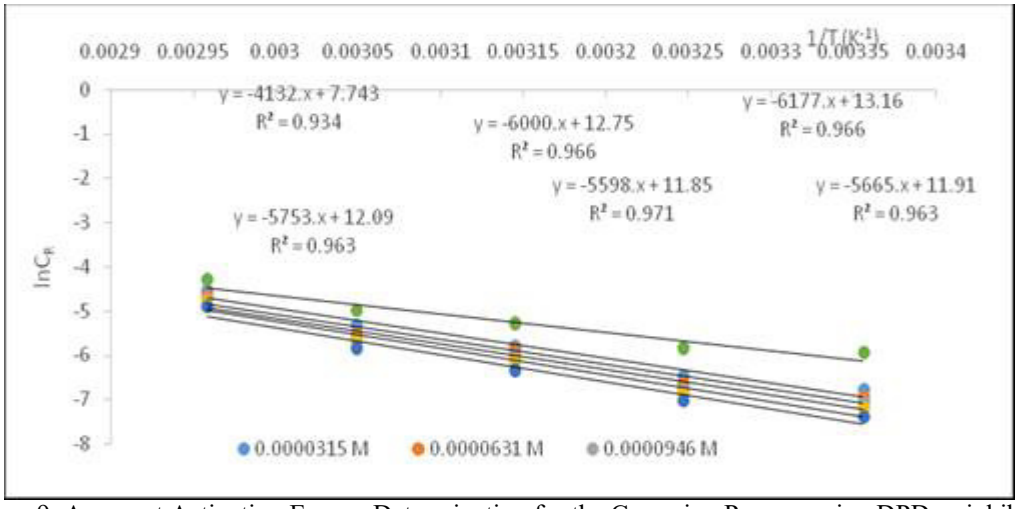


Figure 9: Apparent Activation Energy Determination for the Corrosion Process using DPD as inhibitor

Table 4: Activation energy, Ea and pre-exponential factor A for the corrosion process in 0.5 M HCl

| Compd | Concentration (ppm) | Slope | $E_a$ (J/mol) | lnA | A |
|---|---|---|---|---|---|
| DPD | BLANK | -4133 | 34361.76 | 7.7432 | 2305.839 |
| | 0.0000315 | -5599 | 46550.09 | 11.854 | 140645.8 |
| | 0.0000631 | -5666 | 47107.12 | 11.917 | 149791.6 |
| | 0.0000946 | -5753 | 47830.44 | 12.093 | 178617.2 |
| | 0.0001261 | -6001 | 49892.31 | 12.757 | 346972.2 |
| | 0.0001576 | -6178 | 51363.89 | 13.163 | 520736.8 |

The Apparent activation energies in the presence of different concentration of DPD were greater than that of pure acidic medium indicating that the inhibitor adsorbed on most active adsorption sites with lowest energy while the corrosion takes place mainly on the active sites having higher energy (Tu *et al.,* 2012). An explanation can be given to this end that the corrosion reaction requires higher energies to occur in the inhibited solution than the uninhibited one showing the inhibiting action of DPD. The higher values of $E_a$ also indicate the physiadsorption that occurred in the first stage (Chen *et al.,* 2011; Tu *et al.,* 2012). The pre-exponential factor, A, in the Arrhenius equation is related to the number of active canters. The larger values of A in the presence of DPD compared to that of the uninhibited solution (Table 4) implied that most of the active sites are blocked by the adsorption of the inhibitor (Tu *et al.,* 2012).

The values of enthalpy, ΔH* and entropy, ΔS*of activation were calculated from the slope and intercepts of the plots of $\ln(C_R/T)$ vs. 1/T (Figure 10) using the transition state Equation 9 and the values are given in Table 5.

$$C_R = \left(\frac{RT}{Nh}\right) \times \exp\left(\frac{\Delta S^*}{R}\right) \times \exp\left(\frac{-\Delta H^*}{RT}\right) \quad 9$$

Where h is the Planks' constant, N the Avogadro's number, T the absolute temperature and R the universal gas constant.

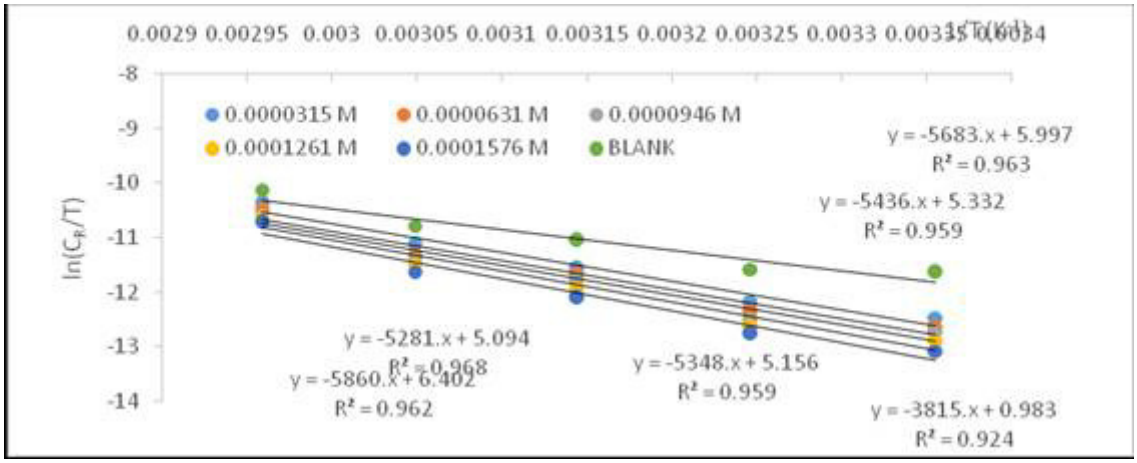


Figure 10: Transition State Determination of Enthalpy and Entropy of Activation using DPD

 

Table 5: Values for the Corrosion Activation Parameters of Mild Steel in 0.5 M HCl in the absence and presence of different Concentration of DPD

| Compd | Conc. (M) | Slope | Intercept | Enthalpy (J/mol) | Entropy ($Jmol^{-1}k^{-1}$) |
|---|---|---|---|---|---|
| DPD | BLANK | -3816 | 0.983 | 31726.224 | -189.3665 |
| | 0.0000315 | -5281 | 5.094 | 43906.234 | -155.18765 |
| | 0.0000631 | -5349 | 5.157 | 44471.586 | -154.6655 |
| | 0.0000946 | -5436 | 5.333 | 45194.904 | -153.2056 |
| | 0.0001261 | -5683 | 5.997 | 47248.462 | -147.6801 |
| | 0.0001576 | -5861 | 6.403 | 48728.354 | -144.3096 |

Table 5 revealed that ΔH* and ΔS* values on addition of DPD to the tested solution are more than that of the uninhibited solution. This implies that the energy barrier of the corrosion rises in the presence of DPD and this is in agreement with the values of activation energy, $E_a$, shown in Table 4.The enthalpies of activation ΔH* are positive both in the absence and presence of DPD indicating endothermic nature of the mild steel dissolution (Szauer and Brandt, 1981; Obot and Obi-Egbedi, 2008; Dahmani *et al.,* 2010; Peme *et al.,* 2015). The negative values of ΔS* using both dyes imply that the formation of the activated complex in the rate determining step represent an associative process rather than dissociative and hence gave a hint of the decrease in disorderliness as the reaction moves from the reactants to the activated complex (Saliyan and Adhikari, 2008; Peme *et al.,* 2015).

### 3.8 Quantum Chemical Calculations

Quantum chemical helps to give information about molecular structure and electrochemical behaviour of molecule. To investigate the adsorption and inhibition mechanism relating to the molecular structure of DPD, Theoretical calculations were employed by DFT method using B3LYP level and 6-31G* basis set. The Optimised structure and frontier molecular orbitals of the investigated DPD azo dye are shown in Figure 11 and the results from the quantum calculation are given by Table 6.

**Table 6**: Quantum chemical parameters for DPD dye.

| Parameters | $E_{HOMO}$(eV) | $E_{LUMO}$(eV) | ΔE (eV) | H | δ (eV) | X | $\omega$ | $\mu$ | ΔN |
|---|---|---|---|---|---|---|---|---|---|
| DPD | -5.75 | -2.69 | 3.08 | 1.54 | 0.64 | 4.21 | 5.15 | 1.38 | 0.90 |

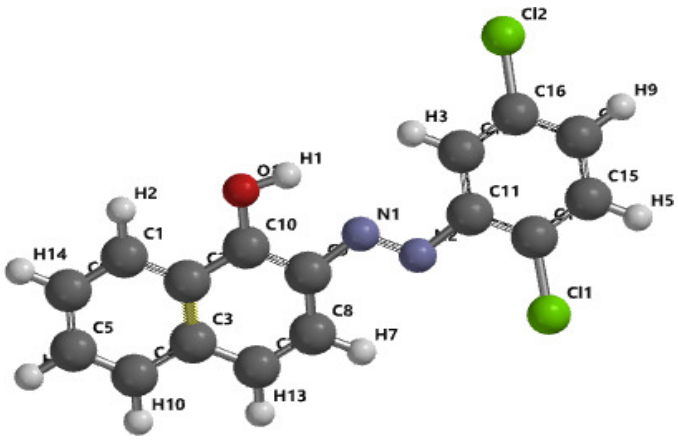


a. Optimised Structu

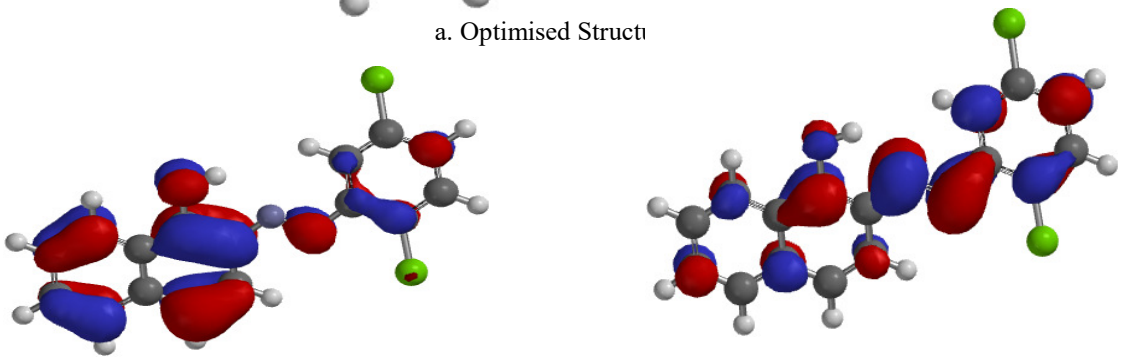

b. HOMO c. LUMO

**Figure 11:** (a) optimized structure, (b) Highest occupied molecular orbital (HOMO) and (c) the Lowest occupied molecular orbital (LUMO) of DPD.

 

According to frontier molecular theory (FMO), the chemical reactivity is a function of interaction between HOMO and LUMO levels of reacting species. HOMO is the site where electron resides, and it provides information about the sites of inhibitor molecule that can most likely donate electrons to the appropriate vacant d-orbital of the metal while LUMO is the vacant orbital for accepting electron(s). The greater the HOMO, the greater is the trend of offering electron to virtual d-orbital of the metal and the lower the LUMO, the easier the acceptance of electrons from the metal surface. The higher value of HOMO (-5.7 5eV) obtained in this study indicates the ability of DPD molecules to donate electron to the appropriate d-orbital of the metal, while the value of its LUMO (-2.67 eV) indicates its ability to accept electron. The higher dipole moment and low energy gap ΔE (3.08 eV) showed that adsorption from DPD molecules to the metal surface takes place thereby reducing the corrosion rates of the mild steel. From the frontier molecule, the HOMO is largely distributed over the C atoms of the aromatic rings, azo-N atoms and the O- atom of the hydroxyl while the LUMO is mainly distributed on the C1, C3, C5, C10, C11, C12, C15 and N.

**4.0 Conclusion**

(E)-2-((2,5-Dichlorophenyl)diazenyl)naphthalen-1-ol (DPD) was synthesized and characterized. From its inhibitory performance evaluated using gravimetric and electrochemical methods, the following deductions could be drawn that DPD is a good inhibitor for mild steel in acidic environment. Its inhibition efficiency is enhanced with increase in its concentration while it decreases with increase in temperature. Electrochemical measurement using potentiodynamic polarization revealed DPD as cathodic type organic inhibitor. Increase in the inhibitory efficiencies of DPD with increase in its concentration observed using gravimetric and electrochemical methods in this study indicates strong agreement of both methods. The adsorption of DPD on mild steel obeys Langmuir adsorption isotherm and is an exothermal and entropy increasing process while the adsorption mechanism follows physical adsorption. The increase in the entropy observed in the study was due to desorption of the already adsorbed water molecule on the mild steel while being substituted for by DPD molecules. The values of activation parameters ($E_a$, ΔH* and ΔS*) increase with increase in DPD concentration. Hence, it could be deduced that the adsorbed DPD molecules blocked the active sites having lower energy thereby inhibiting the effect of the corrosive medium. As been analyzed using quantum chemical method, the main active sites of DPD molecules that enhanced its adsorption on the mild steel surface included the nitrogen atoms of the azo group, oxygen atom of the substituent hydroxyl group and the plane conjugated system i.e. the aromatic rings.

**References**.

Abdallah, M., 2002. Rhodanine azosulpha drugs as corrosion inhibitors for corrosion of 304 stainless steel in hydrochloric acid solution. *Corrosion Science*, *44*(4), pp.717-728.

Ahmadi, R.A. and Amani, S., 2012. Synthesis, spectroscopy, thermal analysis, magnetic properties and biological activity studies of Cu (II) and Co (II) complexes with Schiff base dye ligands. *Molecules*, *17*(6), pp.6434-6448.

Al-Doori, H.H. and Shihab, M.S., 2014. Study of Some [N-substituted] p-aminoazobenzene as Corrosion Inhibitors for Mild-Steel in 1M H2SO4. *Journal of Al-Nahrain University-Science*, *17*(3), pp.59-68.

Anitha, K.R., Venugopala, R. and Rao, V.K.S., 2011. , Synthesis and Antimicrobial Evaluation of Metal (II) Complexes of A Novel Bisazo Dye 2, 2 [benzene-13-diyl di (E) diazene 2, 1-diyl] bis (4-chloroaniline). *J. Chem. Pharm. Res*, *3*(3), pp.511-519.

Ateya, B.G., El-Anadouli, B.E. and El-Nizamy, F.M., 1984. The adsorption of thiourea on mild steel. *Corrosion Science*, *24*(6), pp.509-515.

Cabir, B., Avar, B., Gulcan, M., Kayraldiz, A. and Kurtoglu, M., 2013. Synthesis, spectroscopic characterization, and genotoxicity of a new group of azo-oxime metal chelates. *Turkish Journal of Chemistry*, *37*(3), pp.422-438.

Çanakci, D., Saribiyik, O.Y. and Serin, S., 2014. Synthesis, structural characterization of Co (II), Ni (II) and Cu (II) complexes of azo dye ligands derived from dihydroxy naphthalene. *Inter. J. Sci. Res. Innov. Tech*, *1*, pp.52-72.

Chen, W., Luo, H.Q. and Li, N.B., 2011. Inhibition effects of 2, 5-dimercapto-1, 3, 4-thiadiazole on the corrosion of mild steel in sulphuric acid solution. *Corrosion Science*, *53*(10), pp.3356-3365.

Dahmani, M., Et-Touhami, A., Al-Deyab, S.S., Hammouti, B. and Bouyanzer, A., 2010. Corrosion inhibition of C38 steel in 1 M HCl: A comparative study of black pepper extract and its isolated piperine. *Int. J. Electrochem. Sci*, *5*(8), pp.1060-1069.

Deng, S. and Li, X., 2012. Inhibition by Jasminum nudiflorum Lindl. leaves extract of the corrosion of aluminium in HCl solution. *Corrosion Science*, *64*, pp.253-262.

Durnie, W., De Marco, R., Jefferson, A. and Kinsella, B., 1999. Development of a structure-activity relationship

 

for oil field corrosion inhibitors. *Journal of the Electrochemical Society*, *146*(5), pp.1751-1756.
Ebenso, E.E., Alemu, H., Umoren, S.A. and Obot, I.B., 2008. Inhibition of mild steel corrosion in sulphuric acid using alizarin yellow GG dye and synergistic iodide additive. *Int. J. Electrochem. Sci*, *3*, pp.1325-1339.
Farag, A.A. and Hegazy, M.A., 2013. Synergistic inhibition effect of potassium iodide and novel Schiff bases on X65 steel corrosion in 0.5 M H2SO4. *Corrosion Science*, *74*, pp.168-177.
Fiori-Bimbi, M.V., Alvarez, P.E., Vaca, H. and Gervasi, C.A., 2015. Corrosion inhibition of mild steel in HCL solution by pectin. *Corrosion Science*, (92), pp.192-199.
Fouda, A.S., El-Azaly, A.H., Awad, R.S. and Ahmed, A.M., 2014. New benzonitrile azo dyes as corrosion inhibitors for carbon steel in hydrochloric acid solutions. *Int. J. Electrochem. Sci*, *9*, pp.1117-1131.
Geethamani, P. and Kasthuri, P.K., 2015. Adsorption and corrosion inhibition of mild steel in acidic media by expired pharmaceutical drug. *Cogent Chemistry*, *1*(1), p.1091558.
Hamdy, A. and El-Gendy, N.S., 2013. Thermodynamic, adsorption and electrochemical studies for corrosion inhibition of carbon steel by henna extract in acid medium. *Egyptian Journal of Petroleum*, *22*(1), pp.17-25.
Hasanov, R., Bilge, S., Bilgiç, S., Gece, G. and Kılıç, Z., 2010. Experimental and theoretical calculations on corrosion inhibition of steel in 1 M H2SO4 by crown type polyethers. *Corrosion Science*, *52*(3), pp.984-990.
Hassan, H.H., 2007. Inhibition of mild steel corrosion in hydrochloric acid solution by triazole derivatives: Part II: Time and temperature effects and thermodynamic treatments. *Electrochimica Acta*, *53*(4), pp.1722-1730.
He, X., Jiang, Y., Li, C., Wang, W., Hou, B. and Wu, L., 2014. Inhibition properties and adsorption behavior of imidazole and 2-phenyl-2-imidazoline on AA5052 in 1.0 M HCl solution. *Corrosion Science*, *83*, pp.124-136.
Hegazy, M.A., 2009. A novel Schiff base-based cationic gemini surfactants: synthesis and effect on corrosion inhibition of carbon steel in hydrochloric acid solution. *Corrosion Science*, *51*(11), pp.2610-2618.
Hu, J., Zeng, D., Zhang, Z., Shi, T., Song, G.L. and Guo, X., 2013. 2-Hydroxy-4-methoxy-acetophenone as an environment-friendly corrosion inhibitor for AZ91D magnesium alloy. *Corrosion Science*, *74*, pp.35-43.
Li, X.H., Deng, S.D. and Fu, H., 2010. Inhibition by Jasminum nudiflorum Lindl. leaves extract of the corrosion of cold rolled steel in hydrochloric acid solution. *Journal of Applied Electrochemistry*, *40*(9), pp.1641-1649.
Mu, G., Li, X., Qu, Q. and Zhou, J., 2006. Molybdate and tungstate as corrosion inhibitors for cold rolling steel in hydrochloric acid solution. *Corrosion Science*, *48*(2), pp.445-459.
Nabi, A. S., and Hussain, A. A., 2012. Synthesis, Identification and study of some new azo dyes as corrosion Inhibitors for Carbon-Steel in acidic media. *Journal of Basrah Researches (Sciences)*, *38*(1A), pp.125-146.
Nagiub, A.M., Mahross, M.H., Khalil, H.F.Y., Mahran, B.N.A., Yehia, M.M. and El-Sabbah, M.M.B., 2013. Azo Dye Compounds as Corrosion Inhibitors for Dissolution of Mild Steel in Hydrochloric Acid Solution. *Portugaliae Electrochimica Acta*, *31*(2), pp.119-139.
Obi-Egbedi, N.O., Obot, I.B., El-Khaiary, M.I., Umoren, S.A. and Ebenso, E.E., 2011. Computational simulation and statistical analysis on the relationship between corrosion inhibition efficiency and molecular structure of some phenanthroline derivatives on mild steel surface. *Int. J. Electrochem. Sci*, *6*, pp.5649-5675.
Obot, I.B. and Obi-Egbedi, N.O., 2008. Fluconazole as an inhibitor for aluminium corrosion in 0.1 M HCl. *Colloids and surfaces a: physicochemical and engineering aspects*, *330*(2-3), pp.207-212.
Obot, I.B., Obi-Egbedi, N.O. and Umoren, S.A., 2009. Antifungal drugs as corrosion inhibitors for aluminium in 0.1 M HCl. *Corrosion Science*, *51*(8), pp.1868-1875.
Olasunkanmi, L.O., Obot, I.B., Kabanda, M.M. and Ebenso, E.E., 2015. Some quinoxalin-6-yl derivatives as corrosion inhibitors for mild steel in hydrochloric acid: experimental and theoretical studies. *The Journal of Physical Chemistry C*, *119*(28), pp.16004-16019.
Otutu, J. O., 2013. Synthesis and application of azo dyes derived from 2-amino-1, 3, 4-thiadiazole-2-thiol on polyester fibre. *International Journal of Recent Research and Applied Studies*, *15*(2), pp. 292-296.
Peme, T., Olasunkanmi, L.O., Bahadur, I., Adekunle, A.S., Kabanda, M.M. and Ebenso, E.E., 2015. Adsorption and corrosion inhibition studies of some selected dyes as corrosion inhibitors for mild steel in acidic medium: gravimetric, electrochemical, quantum chemical studies and synergistic effect with iodide ions. *Molecules*, *20*(9), pp.16004-16029.
Qian, B., Hou, B. and Zheng, M., 2013. The inhibition effect of tannic acid on mild steel corrosion in seawater wet/dry cyclic conditions. *Corrosion Science*, *72*, pp.1-9.
Qian, B., Wang, J., Zheng, M. and Hou, B., 2013. Synergistic effect of polyaspartic acid and iodide ion on corrosion inhibition of mild steel in H2SO4. *Corrosion Science*, *75*, pp.184-192.
Quraishi, M.A., 2013. Electrochemical and theoretical investigation of triazole derivatives on corrosion inhibition behavior of copper in hydrochloric acid medium. *Corrosion Science*, *70*, pp.161-169.
Ramachandran, S., Jovancicevic, V.,1999. Molecular Modeling of the Inhibition of Mild Steel Carbon Dioxide Corrosion by Imidazolines. *Corrosion Science*, 55(3), pp. 259-267.
Riggs Jr, O.L. and Hurd, R.M., 1967. Temperature coefficient of corrosion inhibition. *Corrosion*, *23*(8), pp.252-260.

 

Saliyan, V.R. and Adhikari, A.V., 2008. Inhibition of corrosion of mild steel in acid media by N′-benzylidene-3-(quinolin-4-ylthio) propanohydrazide. *Bulletin of Materials Science*, *31*(4), pp.699-711.

Selvaraj, S.K., Micheal, S.M., Dharmalingam, V., Sahayaraj, J.W., Amalraj, A.J., Mohan, R. and Sahayaraj, P.A., 2015. Corrosion Inhibitor 5-Sulpho Salicylic Acid Controlling the Corrosion of Carbon Steel in Well Water. *European Journal of Academic Essays*, *2*(4), pp.1-5.

Solmaz, R., Kardaş, G. and Erbil, M., 2008. Adsorption and corrosion inhibitive properties of 2-amino-5-mercapto-1, 3, 4-thiadiazole on mild steel in hydrochloric acid media. *Colloids and Surfaces A: Physicochemical and Engineering Aspects*, *312*(1), pp.7-17.

Szauer, T. and Brandt, A., 1981. Adsorption of oleates of various amines on iron in acidic solution. *Electrochimica Acta*, *26*(9), pp.1253-1256.

Tu, S., Jiang, X., Zhou, L., Wang, H. and Jiang, X., 2012. Synthesis of N-alkyl-4-(4-hydroxybut-2-ynyl) pyridinium bromides and their corrosion inhibition activities on X70 steel in 5 M HCl. *Corrosion Science*, *65*, pp.13-25.

Wang, B., Du, M., Zhang, J. and Gao, C.J., 2011. Electrochemical and surface analysis studies on corrosion inhibition of Q235 steel by imidazoline derivative against CO2 corrosion. *Corrosion Science*, *53*(1), pp.353-361.

Yıldız, R., 2015. An electrochemical and theoretical evaluation of 4, 6-diamino-2-pyrimidinethiol as a corrosion inhibitor for mild steel in HCl solutions. *Corrosion Science*, *90*, pp.544-553.

Zhang, G., Chen, C., Lu, M., Chai, C. and Wu, Y., 2007. Evaluation of inhibition efficiency of an imidazoline derivative in CO2-containing aqueous solution. *Materials Chemistry and Physics*, *105*(2-3), pp.331-340.